

Main belt asteroids taxonomical information from Dark Energy Survey data

V. Carruba,^{1,2} J. I. B. Camargo,^{3,2} S. Aljbaae,⁴ F. S. Ferreira,^{3,2} E. Lin,⁵ V. Figueiredo-Peixoto,^{3,6,2} M. V. Banda-Huarca,^{3,2} A. Pieres,² R. C. Bouffleur,^{3,2} L. N. da Costa,² T. M. C. Abbott,⁷ M. Agüena,² Sahar S. Allam,⁸ O. Alves,⁵ P. H. Bernardinelli,⁹ E. Bertin,^{10,11} D. Brooks,¹² A. Carnero Rosell,^{13,2,14} J. Carretero,¹⁵ M. E. S. Pereira,¹⁶ T. M. Davis,¹⁷ J. De Vicente,¹⁸ S. Desai,¹⁹ P. Doel,¹² I. Ferrero,²⁰ D. Friedel,²¹ J. Frieman,^{8,22} J. García-Bellido,²³ M. Gatti,²⁴ G. Giannini,¹⁵ D. Gruen,²⁵ R. A. Gruendl,^{21,26} K. Herner,⁸ S. R. Hinton,¹⁷ D. L. Hollowood,²⁷ D. J. James,²⁸ S. Kent,^{8,22} K. Kuehn,^{29,30} O. Lahav,¹² J. L. Marshall,³¹ J. Mena-Fernández,¹⁸ R. Miquel,^{32,15} A. Palmese,³³ A. A. Plazas Malagón,^{34,35} M. Rodríguez-Monroy,³⁶ E. Sanchez,¹⁸ B. Santiago,^{37,2} M. Schubnell,⁵ M. Smith,³⁸ E. Suchyta,³⁹ M. E. C. Swanson,⁴⁰ G. Tarle,⁵ A. R. Walker,⁷ N. Weaverdyck,^{5,41} and P. Wiseman³⁸

(DES Collaboration)

¹ São Paulo State University (UNESP), School of Natural Sciences and Engineering

² Laboratório Interinstitucional de e-Astronomia - LIneA, Brazil

³ Observatório Nacional, Rua Gal. José Cristino 77, Rio de Janeiro, RJ - 20921-400, Brazil

⁴ National Space Research Institute (INPE), Division of Space Mechanics and Control, C.P. 515, 12227-310, São José dos Campos, SP, Brazil

⁵ Department of Physics, University of Michigan, Ann Arbor, MI 48109, USA

⁶ IGeo - Universidade Federal do Rio de Janeiro, Av. Athos da Silveira Ramos 274, Rio de Janeiro, RJ - 21941-916, Brazil

⁷ Cerro Tololo Inter-American Observatory, NSF's National Optical-Infrared Astronomy Research Laboratory, Casilla 603, La Serena, Chile

⁸ Fermi National Accelerator Laboratory, P. O. Box 500, Batavia, IL 60510, USA

⁹ Astronomy Department, University of Washington, Box 351580, Seattle, WA 98195, USA

¹⁰ CNRS, UMR 7095, Institut d'Astrophysique de Paris, F-75014, Paris, France

¹¹ Sorbonne Universités, UPMC Univ Paris 06, UMR 7095, Institut d'Astrophysique de Paris, F-75014, Paris, France

¹² Department of Physics & Astronomy, University College London, Gower Street, London, WC1E 6BT, UK

¹³ Instituto de Astrofísica de Canarias, E-38205 La Laguna, Tenerife, Spain

¹⁴ Universidad de La Laguna, Dpto. Astrofísica, E-38206 La Laguna, Tenerife, Spain

¹⁵ Institut de Física d'Altes Energies (IFAE), The Barcelona Institute of Science and Technology, Campus UAB, 08193 Bellaterra (Barcelona) Spain

¹⁶ Hamburger Sternwarte, Universität Hamburg, Gojenbergsweg 112, 21029 Hamburg, Germany

¹⁷ School of Mathematics and Physics, University of Queensland, Brisbane, QLD 4072, Australia

¹⁸ Centro de Investigaciones Energéticas, Medioambientales y Tecnológicas (CIEMAT), Madrid, Spain

¹⁹ Department of Physics, IIT Hyderabad, Kandi, Telangana 502285, India

²⁰ Institute of Theoretical Astrophysics, University of Oslo. P.O. Box 1029 Blindern, NO-0315 Oslo, Norway

²¹ Center for Astrophysical Surveys, National Center for Supercomputing Applications, 1205 West Clark St., Urbana, IL 61801, USA

²² Kavli Institute for Cosmological Physics, University of Chicago, Chicago, IL 60637, USA

²³ Instituto de Física Teórica UAM/CSIC, Universidad Autónoma de Madrid, 28049 Madrid, Spain

²⁴ Department of Physics and Astronomy, University of Pennsylvania, Philadelphia, PA 19104, USA

²⁵ University Observatory, Faculty of Physics, Ludwig-Maximilians-Universität, Scheinerstr. 1, 81679 Munich, Germany

²⁶ Department of Astronomy, University of Illinois at Urbana-Champaign, 1002 W. Green Street, Urbana, IL 61801, USA

²⁷ Santa Cruz Institute for Particle Physics, Santa Cruz, CA 95064, USA

²⁸ Center for Astrophysics | Harvard & Smithsonian, 60 Garden Street, Cambridge, MA 02138, USA

²⁹ Australian Astronomical Optics, Macquarie University, North Ryde, NSW 2113, Australia

³⁰ Lowell Observatory, 1400 Mars Hill Rd, Flagstaff, AZ 86001, USA

³¹ George P. and Cynthia Woods Mitchell Institute for Fundamental Physics and Astronomy, and Department of Physics and Astronomy, Texas A&M University, College Station, TX 77843, USA

³² Institució Catalana de Recerca i Estudis Avançats, E-08010 Barcelona, Spain

³³ Department of Physics, Carnegie Mellon University, Pittsburgh, Pennsylvania 15312, USA

³⁴ Kavli Institute for Particle Astrophysics & Cosmology, P. O. Box 2450, Stanford University, Stanford, CA 94305, USA

³⁵ SLAC National Accelerator Laboratory, Menlo Park, CA 94025, USA

³⁶ Laboratoire de Physique des 2 Infinis Irène Joliot-Curie, CNRS Université Paris-Saclay, Bât. 100, Faculté des sciences, F-91405 Orsay Cedex, France

³⁷ Instituto de Física, UFRGS, Caixa Postal 15051, Porto Alegre, RS - 91501-970, Brazil

³⁸ School of Physics and Astronomy, University of Southampton, Southampton, SO17 1BJ, UK

³⁹ Computer Science and Mathematics Division, Oak Ridge National Laboratory, Oak Ridge, TN 37831

⁴⁰ Independent Researcher

⁴¹ Lawrence Berkeley National Laboratory, 1 Cyclotron Road, Berkeley, CA 94720, USA

ABSTRACT

While proper orbital elements are currently available for more than 1 million asteroids, taxonomical information is still lagging behind. Surveys like SDSS-MOC4 provided preliminary information for more than 100,000 objects, but many asteroids still lack even a basic taxonomy. In this study, we use Dark Energy Survey (DES) data to provide new information on asteroid physical properties. By cross-correlating the new DES database with other databases, we investigate how asteroid taxonomy is reflected in DES data. While the resolution of DES data is not sufficient to distinguish between different asteroid taxonomies within the complexes, except for V-type objects, it can provide information on whether an asteroid belongs to the C- or S-complex. Here, machine learning methods optimized through the use of genetic algorithms were used to predict the labels of more than 68 000 asteroids with no prior taxonomic information. Using a high-quality, limited set of asteroids with data on gri slopes and $i - z$ colors, we detected 409 new possible V-type asteroids. Their orbital distribution is highly consistent with that of other known V-type objects.

Key words: Minor planets, asteroids: general, catalogues, celestial mechanics.

1 INTRODUCTION

Currently, we know more than 1 million asteroids for which synthetic proper elements can be reliably obtained using the method of Knežević & Milani (2003). Unlike osculating elements, proper elements are constants of motion on timescales of Myr, which allows for the identification of asteroid families. Our knowledge of the physical properties of asteroids is, however, much more limited. A full spectral classification of asteroids is available in various surveys for slightly more than 2000 objects (Bus & Binzel 2002; Lazzaro et al. 2004; DeMeo et al. 2009). Preliminary taxonomical information can be obtained from surveys like the SDSS-MOC4 (Ivezić et al. 2001), using the method described in DeMeo & Carry (2013), for more than 100,000 asteroids. More recent works on the matter are those of Popescu et al. (2018) on the taxonomic classification of asteroids based on MOVIS near-infrared colors, and the new 3D machine learning classification scheme based on SDSS-MOC4 data of Roh et al. (2022). Yet, many objects, especially those at higher magnitudes and smaller diameters, lack any physical information. This limits studies on asteroid families, which are assumed to be mostly uniform in physical properties.

Asteroids can be classified into three main taxonomical groups based on their reflectance spectra. Asteroids belonging to the C-complex are typically dark in color and have low albedos (reflectivity), while S-complex asteroids are typically brighter and more reflective. In the DeMeo & Carry (2013) taxonomy, the X class is divided into three classes, E, M, and P, which are distinguished solely by their albedo ($P < 0.075$, $0.075 < M < 0.30$, $E > 0.30$). V-type asteroids are characterized by a deep absorption band around 1 micrometer, which is thought to be caused by the presence of the mineral olivine. They are thought to originate from the mantle of differentiated parent bodies.

The Dark Energy Survey (DES; Flaugher 2005, see also Dark Energy Survey Collaboration et al. (2016)) is used here to provide additional information on a set of more than 60,000 asteroids. DES is a collaborative effort that covered 5000 square degrees of the sky in the $grizY$ bands from 2013 to 2019, primarily in the southern celestial sphere, aiming

at investigating the dark energy. It is clear, however, its importance as also a Solar System survey. In fact, among its contributions, DES discovered and characterized a large and distant scattered disk object (Gerdes et al. 2017), improved predictions of stellar occultations by numerous TNOs and Centaurs (Banda-Huarcá et al. 2019), made hundreds of discoveries in the TNO region (Bernardinelli et al. 2022), provided a detailed photometric analysis of a large sample of Jupiter Trojans (Pan et al. 2022), produced the largest TNO color and light curve catalog, facilitated the development of techniques to obtain optimal measurements of fluxes, colors, binarity, and variability for these slow-moving objects (Bernardinelli et al. 2023), and even discovered a messenger from the outskirts of the Solar System (Bernardinelli et al. 2021).

We used two sets of data from DES photometric measurements, a high-quality set with gri slopes and $i - z$ colors, where the classification method of DeMeo & Carry (2013) can be applied, and a much larger ($g - r, g - i$) database. We then cross-referenced the DES data with taxonomical, SDSS-MOC4, and albedo information, to understand how asteroid taxonomies are mapped in the new dataset. Based on the distribution of known asteroid taxonomies, predictions on unlabeled bodies can then be made, using machine learning methods, optimized by the use of genetic algorithms (Chen, P. W. and Wang, J. Y. and Lee H. 2004). Special attention is then given to more robust taxonomical classification for asteroid taxonomies that showed a good performance in DES data, such as the important V-type asteroids.

In section 2, we describe how the data was obtained from the DES database and organized. In section 3, we describe the use of the DeMeo and Carry taxonomy. Studies using the ($g - r, g - i$) data are done in section 4. Section 5 presents DES candidates for V-type asteroids, and conclusions are given in section 6.

2 OBTAINING DES DATA

All colors presented in this study were obtained through observations and measurements conducted by DES.

To search for known Solar System objects, we queried the entire DES database (Abbott et al. 2021a) using keywords from image headers like pointing coordinates, date and time of observations (Diehl et al. 2023), exposure time, and filter (Flaugher et al. 2015). We used an SQL-based tool called *easyaccess* (Carrasco Kind et al. 2018) for all queries of the DES database.

Having those pieces of information in hand, we identify the single-epoch CCDs that could have captured the image of a small Solar System body using the Sky Body Tracker (SkyBoT; Berthier et al. (2006)). SkyBoT, among other functionalities, yields a list of all known Solar System objects within a given field of view (FOV) when pointing coordinates, UTC date and time of observation, observing site coordinates, and FOV angular size are provided. We selected objects whose dynamical classification, as provided by the SkyBoT, were Hungaria, MB>Inner, MB>Middle, MB>Outer, MB>Cybele, MB>Hilda, or Jupiter Trojan, where MB stands for Main Belt.

We obtained positions, magnitudes and other pieces of information of the selected objects from the Year-6 (Y6) list of objects so-called Y6A1_FINALCUT_OBJECTS. The respective zero-points of each CCD were added to the magnitudes using the Forward Global Calibration Method (Burke et al. 2018), prepared by the collaboration (refer to Sects. 1 and 4.8 in Morganson et al. 2018, for more details about the finalcut catalog).

Methods for improved photometry, applied to outer Solar System objects present in the images of DES, have been recently developed (Bernardinelli et al. 2023). However, the Y6 catalog has features that make it an extremely attractive and valuable source to a variety of photometric studies, the one presented here in particular: (i) the same methods/procedures are used to derive flux measurements over the whole survey area, allowing us to coherently correlate colors of objects from different sky regions and (ii) readily available (upon password) data, thus saving a lot of CPU time, in addition to (iii) high quality single epoch photometry.

Table 1 shows the total number of asteroids that SkyBoT identified as belonging to a DES frame. We selected objects classified as Hungaria ($1.0 < a < 2.0$ au and $a(1 - e) > 1.666$ au), Inner Main Belt ($2.0 \leq a < 2.5$ au), Middle Main Belt ($2.5 \leq a < 2.82$ au), Outer Main Belt ($2.82 \leq a < 3.27$ au), (Main Belt) Cybele ($3.27 \leq a < 3.7$ au), Hilda ($3.7 \leq a < 4.6$ au) and Trojan ($4.6 \leq a < 5.5$ au) according to the SkyBoTclassification¹. However, not all of them were detected, often due to a faint magnitude that is difficult to observe in a single-epoch image or to a very large (many degrees in some cases) positional uncertainty. A brief description of the task and tools used to find known Solar System objects in DES images can be found in the work by Banda-Huarca et al. (2019). All positions and magnitudes were obtained from the Y6 final cut DES catalogs and were queried using the *easyaccess* tool.

It is important to note that the DES observational cadence may not always be suitable for determining the colors of small objects, since observations of a same object in different filters may be separated by long periods of time and

Table 1. Known Main Belt, Hungaria and Trojan objects in DES images as indicated by the SkyBoT. Note that the number of objects effectively present in the images is smaller.

Class	Number of objects
Hungaria	12 199
Main Belt - Inner	102 979
Main Belt - Middle	134 277
Main Belt - Outer	125 823
Cybele	1 876
Hilda	1 751
Trojan	1 684

we do not have accurate enough rotational information to correct for rotational effects. As a result, we formed colors for a given object using only observations that were obtained within 10 minutes of each other (Abbott et al. 2021b).

If we were to conduct an observational run specifically dedicated to measuring the colors of small objects, 10 minutes would be a reasonable estimate for obtaining magnitudes in different filters, taking into account the exposure time, readout and filter change. However, a very fast rotator would likely require simultaneous observations in the different filters.

The ALCDEF (Asteroid Light Curve Data Exchange Format, see Stephens & Warner 2018; Warner et al. 2011; Stephens et al. 2010) website displays a plot² indicating that most asteroids have rotational periods longer than 2 hours, with many falling between 4 and 10 hours. If we consider the shortest period of 2 hours, 10 minutes of observations corresponds to a rotation of 30 degrees, while for a 7-hour period, we have a rotation of only 8.6 degrees. Therefore, our decision to group observations of the same object that were acquired within 10 minutes appears to be a good compromise between minimizing the impact of rotational effects on colors while keeping a sample as large as possible.

We can estimate the maximum error caused by neglecting pure rotational effects (i.e., considering a surface with homogeneous albedo) in our database. If we simplify the asteroid light curves as a double-peaked triangle wave and assume a large amplitude, of 0.5 mag for a 4-hour rotation period, a 10-minute separation between observations corresponds to a magnitude change of approximately $10/(4 \cdot 60/4) \cdot 0.5 \simeq 0.083$. For a 10-hour rotation period, the magnitude change would be only 0.033. Fast-rotating asteroids ($\simeq 4$ hr period) would generally have smaller amplitudes because elongated objects are more prone to breaking (see Figure 9 in Chang et al. (2019)). In most cases, the rotational effect on color should be of the order of 10^{-2} , and should not exceed 0.1.

Albedo variations, however, do exist and have statistical significance on color variations (see discussion in Szabó et al. (2004)). Its overall impact can be inferred from table (2). The color of a given object (e.g., $g - r$) is determined by the mean value of multiple measurements of that color and its uncertainty is represented by the respective standard deviation. One might reasonably anticipate that color uncertain-

¹ <https://vo.imcce.fr/webservices/skybot/?documentation>

² https://alcdef.org/php/alcdef_aboutLightcurves.html

Table 2. DES ($g-r$) colors for inner main belt asteroids. We report the standard deviations of measurements in ($g-r$), the number of colors recorded per object, and the total count of ($g-r$) measurements used to calculate the mean value. Additionally, we present the total count of objects with a ($g-r$) color, regardless whether they were utilized in this study.

Stand. Dev in ($g-r$)	# of ($g-r$) colors per object	Total number of ($g-r$) colors used
0.041	1 to 3	20825
0.058	4 to 6	403
0.059	7 to 9	30
0.064	10 to 12	32
0.051	13 to 15	7
0.028	16 to 18	10
0.044	19 to 21	5
0.042	22 or more	7

ties in color depend on the number of measurements under the influence of a variable albedo (the smaller the average over a rotation, the more probable it is to obtain a large uncertainty). Table (2) shows that this is not the case. Based on this analysis, it can be concluded that albedo variations on the surface of asteroids are not likely to introduce significant systematic effects on our results.

Finally, in order to compare our data with known sources in the literature on asteroid taxonomy (see Sects. 3 and 4), we transformed DES colors into SDSS (Sloan Digital Sky Survey) ones using the transformation equations from [Abbott et al. \(2021a\)](#).

However, instead of using individual equations for each filter, we used their differences. In this context, to provide the necessary photometric information for section 3 and 4, we only needed the following colors from DES: ($g-r$)_{DES}, ($g-i$)_{DES}, ($r-i$)_{DES} and ($i-z$)_{DES}. Solar apparent magnitudes and central wavelengths in the SDSS, where necessary, were taken from [Willmer \(2018\)](#). More specifically, the DES to SDSS color transformations used were

$$\begin{aligned}
 (g-r)_{\text{SDSS}} &= (g-r)_{\text{DES}} + 0.060 \times (g-i)_{\text{DES}} \\
 &\quad - 0.150 \times (r-i) - 0.019 \\
 (g-i)_{\text{SDSS}} &= 1.060 \times (g-i)_{\text{DES}} - 0.167 \times (r-i)_{\text{DES}} \quad (1) \\
 &\quad + 0.022 \\
 (i-z)_{\text{SDSS}} &= (i-z)_{\text{DES}} + 0.113 \times (r-i) - 0.003
 \end{aligned}$$

, where the first members of Eqs. 1 are SDSS colors and colors in the second members are from DES. The variances (σ^2) in SDSS colors are given by the error propagation of these equations, added quadratically the root mean square of the respective band transformations from [Abbott et al. \(2021a\)](#) used to determined each of the color equations above.

3 DES DATABASE: DEMEO AND CARRY TAXONOMY

As a preliminary step of our analysis, we selected asteroids from the DES database for which both gri slopes and $i-z$ colors are both available. The color indices contain information that can be used to derive a very low-

resolution reflectance spectrum denoted as Rf . We calculate Rf using the equation $Rf = 10^{-0.4(M_f - M_{\odot f})}$, where M_f is the magnitude of the asteroid and $M_{\odot f}$ is the magnitude of the Sun in the same filter. To normalize Rf to 1 at a given wavelength we use the relationship $Rf, v = 10^{-0.4[(M_f - M_v) - (M_{\odot f} - M_{\odot v})]}$. The spectral gradient, or slope, is then given by (with λ in nanometers, see also [Sabater et al. \(2009\)](#)):

$$S(\lambda_1, \lambda_2) = 10^4 \frac{Rf_{2,v} - Rf_{1,v}}{|\lambda_2 - \lambda_1|}. \quad (2)$$

In our case, v is the SDSS g filter.

This slope, as given above, is expressed as a percentage per 100 nanometers. To calculate the Rf, v value for each asteroid, we used the Sloan g , r , and i magnitudes and the effective wavelengths (see [Willmer 2018](#)) of each of these filters and then fit a straight line to the pairs (λ, Rf, v) . The angular coefficient from this adjustment gives the gri slope in % / 100nm.

These parameters are necessary to classify the asteroid taxonomies according to the method of [DeMeo & Carry \(2013\)](#), which is based on data from the Sloan Digital Sky Survey-Moving Object Catalog data (SDSS-MOC4; [Ivezić et al. \(2001\)](#)). Our objective here is to identify asteroids present in both catalogs and to infer what taxonomical properties can be obtained from DES data. Given their temporal constraints, 17154 asteroids with gri slopes and $i-z$ colors are present in the DES database. To eliminate outliers, we only consider asteroids within the 0.15 to 0.85 quantile interval for both parameter distributions³. This corresponds to intervals in gri slope between -34.738 and 43.466, and in $i-z$ between -0.627 and 0.612. Outliers are displayed as blue full transparent circles in figure (1). For statistical reasons, we will exclude outliers from our analysis, hereafter, yielding a sample of 17135 asteroids, 10685 of which are numbered, and the rest multi-opposition asteroids. Most of the outliers are data points beyond the range for which the [DeMeo & Carry \(2013\)](#) method applies, shown as a dashed blue box in figure (1), and most of them are not shown in figure (1). Therefore, removing these objects does not cause any significant loss of information⁴. The range of absolute magnitudes for the data set without outliers goes from 9.0 to 20.5. On the top and right side of figure (1), we display histograms of gri slope and $i-z$ colors for the population of asteroids without outliers. While there is a single peak for the $i-z$ distribution, neither distribution is normal. If we compute the skewness, which is a measure of the symmetry or asymmetry of a distribution, and the kurtosis, which measures whether the data are heavy-tailed or light-tailed

³ Quantiles are cut points that divide the range of a probability distribution into continuous intervals with equal probabilities. The median value of a distribution would correspond to a quantile of 0.50. More information on the procedure to compute quantiles can be found in [Blitzstein & Hwang \(2019\)](#).

⁴ Other quantile intervals were also considered. For a distribution within the 0.10 to 0.90 quantile interval only 2 outliers were found. This number increases to 42 if we consider distributions within 0.20 and 0.80. However, for such distributions, some data points within the range for which the classification method proposed by [DeMeo & Carry \(2013\)](#) applies were also excluded. For these reasons, we decided to work with the 0.15 to 0.85 quantile interval.

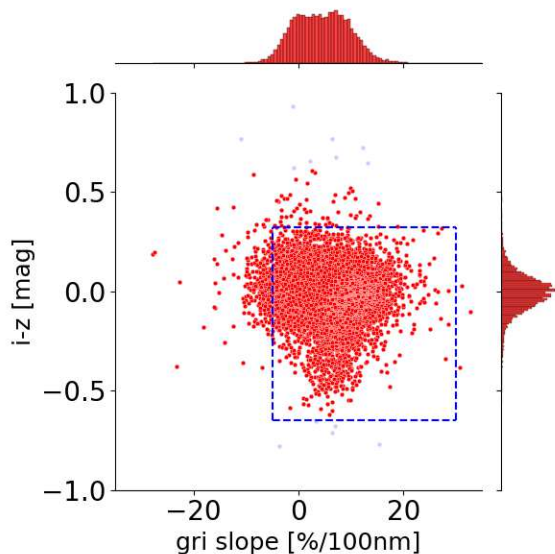


Figure 1. A joint plot of asteroids with available DES data, showing their gri slope, $i - z$ values (blue transparent full circles). The full red circles represent asteroids with values of the two parameters within the 0.15 to 0.85 quantile interval in the gri slope and $i - z$ color distributions. The dashed blue box displays the interval for which the DeMeo & Carry (2013) classification scheme applies. The top and right side of the figure show histograms of the gri slope and $i - z$ colors distributions without outliers, respectively.

relative to a normal distribution, both distribution moments are significantly different from 0, which is the expected value for a Gaussian distribution. Both are skewed, one toward the right and one toward the left flank, with values of skewness of 0.14 and -0.53, respectively. Both are leptokurtic distributions, with heavier tails than a normal distribution. The values of kurtosis are 3.31 and 6.45, respectively. These results show that neither of the distributions can be modelled as Gaussian distributions, and that more complex models should be used for this data.

Having obtained the data set of asteroids in the $(gri$ slope, $i - z$) plane, it may be important to check how properties like the asteroids' absolute magnitudes may correlate with these data. While the size of an asteroid also depends on its albedo, objects with small absolute magnitudes tend to have larger sizes, and vice versa. In the main belt, more than 40% of the asteroid population belong to asteroid families (Milani et al. 2014), and the distribution of large and small objects tends to be not significantly different in proper element domains (Granvik et al. 2017). This is also observed in the $(gri$ slope, $i - z$) plane, as shown in the left panel of figure (2), where the distributions of large and small objects are fairly similar. While smaller objects cover a larger area than the larger ones, this is likely due to their greater number. Regions with a high number density of asteroids are inhabited by both small and large objects. Also, DES data observed fainter objects than previous surveys, like the Sloan Digital Sky Survey-Moving Object Catalog data (SDSS-MOC4 or SDSS, for brevity; Ivezić et al. (2001)). The right panel of figure (2) shows histograms of absolute magnitude distributions for the two surveys. Absolute mag-

nitude H were obtained from the Asteroid Families Portal AFP ("http://asteroids.matf.bg.ac.rs/fam/index.php", Radović et al. (2017), accessed on June 2023). Nominal errors on H are of the order of one decimal digit (Pravec et al. 2012)⁵. We expect that the new data on fainter objects observed by DES could provide new insights on the physical properties of small asteroids.

To begin, we aim at finding location of asteroids with known taxonomies in this new data set. For this purpose, we refer to the asteroid taxonomical data available in the surveys of Bus & Binzel (2002), Lazzaro et al. (2004), and DeMeo et al. (2009). For asteroids with more than one entry in the three surveys, we use a majority vote method to assign the most likely spectral type. There were 14 asteroids with taxonomical data in our selected DES data: 5 C-type, 3 S-type, and 6 X-type. Their location in the $(gri, i - z)$ diagram is shown in figure (3). Apart from two X-type asteroid, there is no indication that the DES parameters are inconsistent with the classification scheme of DeMeo & Carry (2013). However, small number statistics prevent us from reaching more compelling conclusions. Most of the errors that we observed are in the horizontal axis, which are associated to errors in the gri slopes.

To increase the number of asteroids with taxonomical information, we turned our attention to the Sloan Digital Sky Survey-Moving Object Catalog data (SDSS-MOC4; Ivezić et al. (2001)). Although the taxonomical information from the SDSS-MOC4 data has some limitations, as it is based on photometrical colors, it can still provide useful preliminary information on asteroids' physical properties. Firstly, we eliminate asteroids with large errors in gri slope (error larger than 10 %/100nm) and $i - z$ color (error larger than 0.1 mag). Then, we identify 950 asteroids for which the method of DeMeo & Carry (2013) can be used to obtain asteroid taxonomies. Results for the whole SDSS-MOC4 data are available at <https://sbn.psi.edu/pds/resource/sdsstax.html>. The identified asteroids include: 100 X-types, 54 D-types, 345 C-types, 151 L-types, 29 Q-types, 271 S-types, 5 A-types, and 32 V-types. We neglected subclasses like the CX, SQ, SV, LS and QV, since we will show that DES data does not have the resolution needed to perceive these subtle differences. SV and QV objects were classified as V-type since they are all found in regions of the $(gri$ slope, $i - z$) plane occupied by this class of objects. The left panel of figure (4) displays the position in the plane of $i - z$ color versus gri slope for all these asteroids.

The classification obtained from DES data does not always agree with that from SDSS-MOC4, also because the usually large uncertainties on DES gri slopes. To further check the validity of the DES taxonomy, we also performed correlations with the Carvano et al. (2010) and (Popescu et al. 2018) data sets. Table (3) presents the classification accuracy for asteroids in various spectral types for

⁵ The same authors found that there is a systematic negative offset of absolute magnitudes in catalogs, which reaches a peak of -0.5 around $H = 14$. We are not correcting for these biases in this work, since our focus is on larger values of H . However, it is important to alert the reader to these biases for data around $H \simeq 14$.

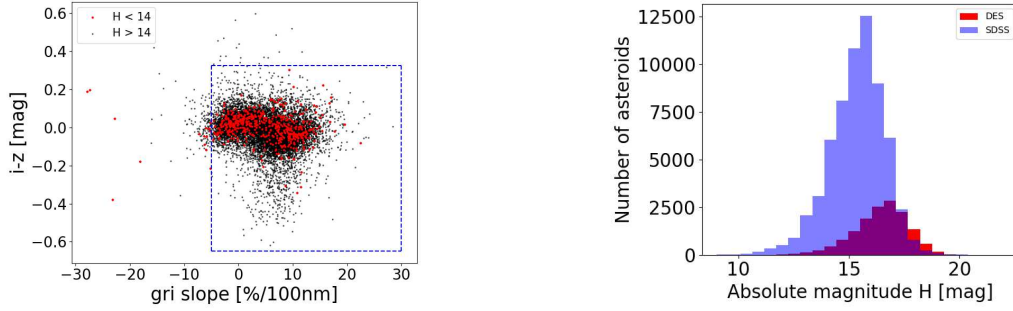


Figure 2. Left panel: a projection in the (gri slope, $i - z$) plane of DES large ($H < 14$) and small ($H > 14$) asteroids. The distribution of the two populations is not significantly different. In the right panel, we show the absolute magnitude distribution of asteroids in the SDSS-MOC4 database and in the DES data set, for which gri slope and $i - z$ colors are available. The DES survey covers fainter objects than those reached by the SDSS one.

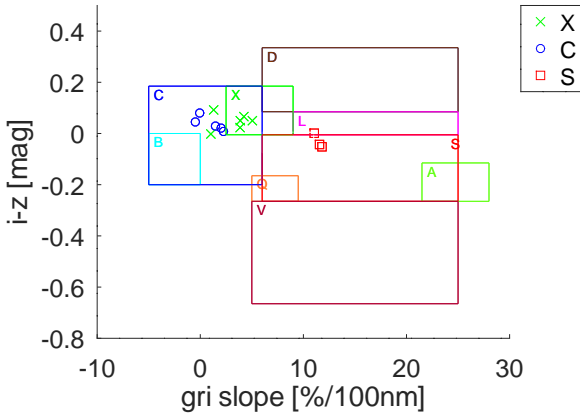


Figure 3. $i - z$ colors versus gri slope for asteroids with taxonomical data present in the DES database. The colored boxes represent the boundaries of the DeMeo & Carry (2013) taxonomical classes.

cross-correlations with the three data sets: C-types and V-types can be classified by DES data with purities, defined as the fraction of DES taxonomic labels correctly classified as such, as of 50% or higher, while the other types have low purity percentages. Interestingly, 44.4% of the misclassified V-type are found in the central and outer main belt, while no confirmed V-type has been found in these regions. This suggests that V-type candidates identified from DES data in these areas should be approached with caution. SV types can be easily misclassified as V-types using DES data, and none of the A-types were classified correctly. Based on this analysis, we propose a limited DES taxonomical classification consisting of three groups, the C- and S-complex, and the V-types. The C-complex will include X, D, and C-types, while the S-complex will encompass the remaining A, L, Q, K, and S-types. The V-types will remain as a separate class.

The new results for DES data are presented in the right panel of figure (4) and table (4). The purities for both complexes are now above 75.0%, suggesting that this simplified scheme could be applied more successfully. Following the analysis of Ivezić et al. (2002), we also plot in figure (5) the orbital distribution of C-complex, S-complex, and V-type objects as identified in both DES and SDSS-MOC4. Proper elements were obtained from AFP. As expected, C-complex asteroids are more common in the outer main belt,

while S-complex asteroids are mostly found in the inner main belt, with some mixing of the two complexes. We can easily identify single asteroid families, like the S-complex Eunomia family in the central main belt, roughly at $a \simeq 2.6$ au, $\sin(i) \simeq 0.25$, or the Koronis family in the pristine region, at $a \simeq 2.9$ au, $\sin(i) \simeq 0.05$. V-type asteroids are mostly associated with the Vesta family at $a \simeq 2.35$ au, $\sin(i) \simeq 0.12$, but are also found in the central and outer main belt. Because of the importance of V-type asteroids for early scenarios of the Solar System formation, we will further discuss their orbital distribution in section (5).

Finally, we searched for objects in the DES dataset with albedo data in the WISE and NEOWISE, AKARI, or IRAS databases (Masiero et al. 2012; Usui et al. 2011; Ryan & Woodward 2010), and we identified 1573 asteroids, as shown in figure 6. Albedo data correlates rather well with the position of asteroids in the plane of $i - z$ color vs gri slope: 81.5% of objects identified as C-complex have values of $p_V < 0.12$, and 94.6% of S-complex asteroids (we include V-type asteroids as S-complex bodies for albedo purposes) have $p_V > 0.12$, as expected for these bodies. The lower value of C-complex asteroids with low albedo data, in contrast to the higher percentage of S-complex asteroids with high albedos can be attributed to the fact that C-complex asteroids include X-type, which, as discussed in section (1), also include the M- and E-types, which have high albedos. Table (5) summarizes our findings.

What predictions can be made based on these results? Based on the results of the SDSS-MOC4 analysis, we can train machine learning (ML) algorithms. In order to select the best-performing ML methods and the combination of its free parameters, or hyper-parameters, that work best for our dataset, we use genetic algorithms (Chen, P. W. and Wang, J. Y. and Lee H. 2004), according to the procedure described in Carruba et al. (2021). We run the genetic algorithm procedure on a subset of asteroids with both DES and SDSS-MOC4 data three times, using a validation set corresponding to 20% of the training data. The use of a validation set is recommended to avoid the issue of overfitting, which happens when the model is overly sensitive to the fine details of the training set, but may perform poorly when dealing with other sets of data. The best-performing algorithm was a Gaussian Naive Bayes (GNB) estimator (Chan et al. 1979). GNB is a classification technique used in ML based on the probabilistic approach and Gaussian

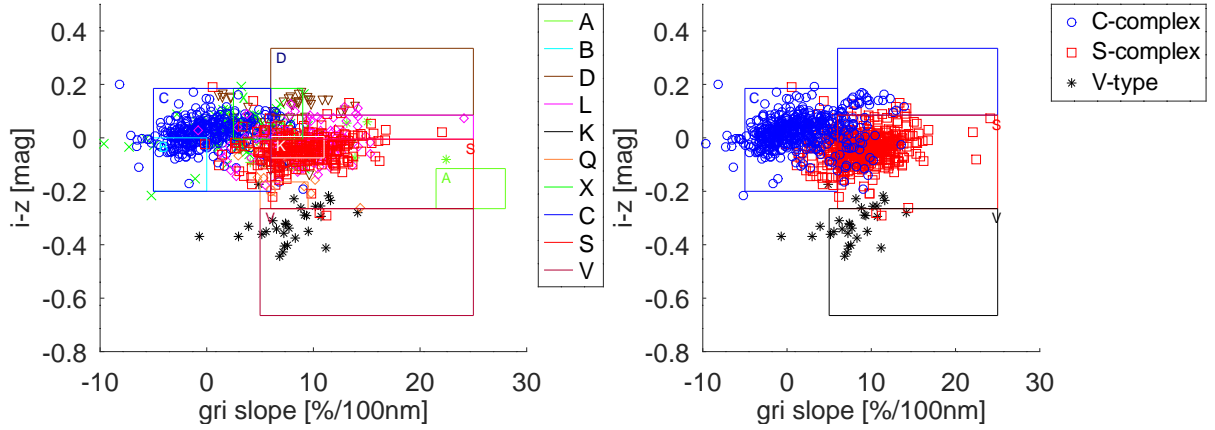


Figure 4. $i - z$ color versus gri slope of asteroids with data in both the SDSS-MOC4 and DES database. The boundaries of the DeMeo & Carry (2013) taxonomical classes are identified by the colored boxes. The left panel displays the positions of these asteroids for all DeMeo & Carry (2013) available classes, while the right panel shows a simplified classification scheme that only identifies C-complex, S-complex asteroids, and V-type objects.

Table 3. Percentage of consistent taxonomic classifications, or purity, for asteroids in both the DES and SDSS-MOC4, the DES and the Carvano et al. (2010), and the DES and the MOVIS databases.

Ast. type	# of asteroids	Percentage of SDSS-MOC4 cons. classification	# of asteroids	Percentage of Carvano et al. (2010) cons. classification	# of asteroids	Percentage of MOVIS cons. classification
X	100	41.0	91	40.7	9	22.2
D	54	37.0	40	30.0	8	12.5
C	345	63.8	335	64.2	21	66.7
A	5	0.0	5	0.0	65	0.0
L	151	19.2	150	18.8	28	32.0
Q	29	34.5	33	30.3	0	-
S	268	38.8	270	38.5	55	34.5
V	32	65.6	25	64.0	21	52.4

Table 4. Percentage of consistent taxonomic classifications (purities) for asteroids in both the DES and SDSS-MOC4 databases for a revised taxonomical scheme.

Asteroid complex	# of asteroids	Percentage of cons. classification
C	499	94.2
S	454	80.0
V	32	65.6

Table 5. Percentage of asteroids with C and S-complexes classifications with geometric albedo $p_v < 0.12$ and $p_v > 0.12$, respectively.

Asteroid complex	# of asteroids	Percentage of albedo values
C	1188	81.5
S	385	94.6

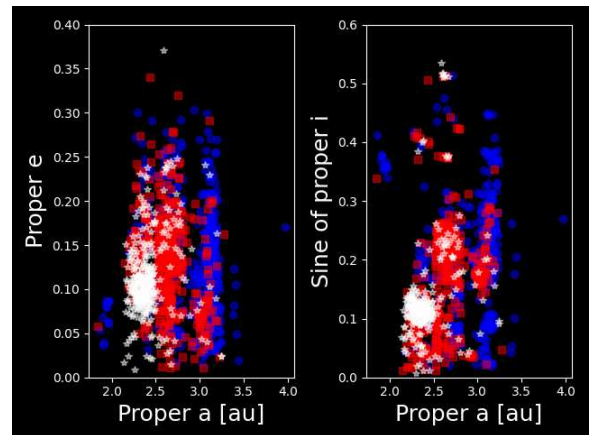


Figure 5. Projections in the proper (a, e) and proper ($a, \sin(i)$) of the C-complex (blue circles), S-complex (red squares) and V-type objects (white asterisks), identified in both the DES and SDSS-MOC4 databases, and as listed in table (4). Proper elements were obtained from *AFP*.

distribution. GNB assumes that each parameter (also called features or predictors) has an independent capacity of pre-

dicting the output variable. The combination of the prediction for all parameters is the final prediction, that returns a probability of the dependent variable to be classified in each group. The final classification is assigned to the group with

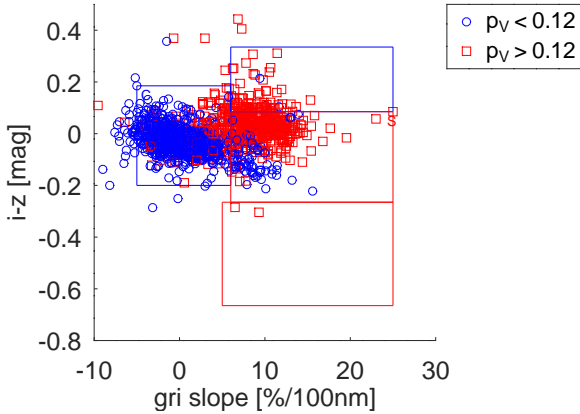


Figure 6. $i - z$ color versus gri slope for asteroids with albedo data and present in the DES database.

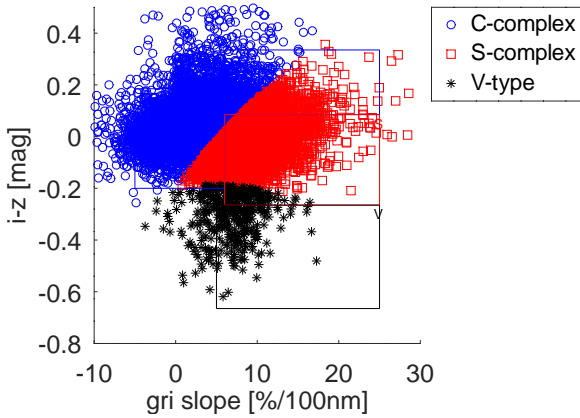


Figure 7. $i - z$ color versus gri slope of the ML predicted data for asteroids in the DES database with no SDSS-MOC4 data.

the higher probability. Finally, since we are dealing with a multi-classification problem, the use of a f_1 score, defined as a harmonic of precision and recall ($f_1 = 2 \cdot \frac{\text{Precision} \cdot \text{Recall}}{\text{Precision} + \text{Recall}}$), is more appropriate to correctly estimate the efficiency of the algorithm, rather than the more commonly used accuracy. The model had an f_1 score of 91.6%.

Figure (7) displays the results of a prediction for 16516 asteroids with no previous labels. Predictions were made separately for numbered and multi-opposition asteroids, using the same training data. The diagonal line in figure (7) is caused by the presence of D-type objects that extends the boundaries of C-complex upward and rightward. In the ML model, this causes the boundary between C-complex and S-complex to be a diagonal line. Our classifier predicts that 10213 of the asteroids are likely to be C-complex, 5890 are likely S-complex asteroids, and 410 are new possible V-type objects.

4 DES DATABASE: (G-R,G-I) PLANE

The number of asteroids with DES data increases significantly if we consider the $g - r$ and $g - i$ colors instead of the $i - z$ and gri slope, passing from 17078 to 61493. Their distribution in the $(g - r, g - i)$ plane is shown in figure 8, with g, r, i being the photometric bands of the SDSS ‘*ugriz*’ sys-

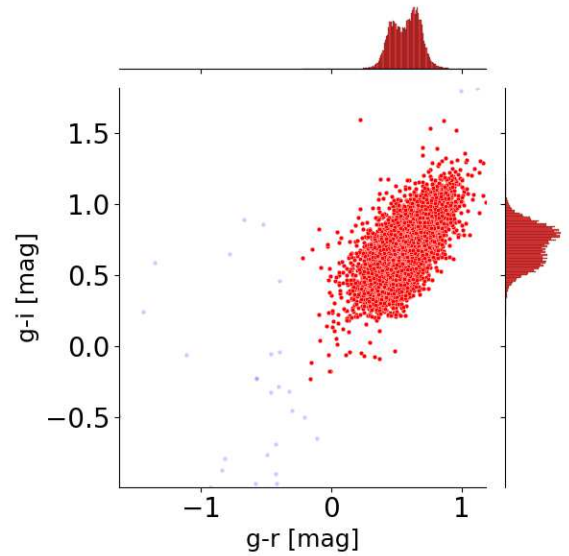


Figure 8. A joint plot of the $(g - r, g - i)$ colors for asteroids with available DES data. The blue full transparent circles indicate outlier data in the distributions of both colors. The histograms of the two colors distributions, without the outliers, are displayed on the top and right sides, respectively.

tem. While some of the brightest objects can have negative values of these colors, most asteroids are found in an interval from 0.2 to 1.2 in both quantities. To eliminate these outliers, we again only consider asteroids within an interval of quantiles of 0.15 to 0.85 for both color distributions, which corresponds to the interval $-0.266 < g - r < 1.393$ and $-0.326 < g - i < 1.746$. Outliers are displayed as blue full circles in the figure, while red full circles show the positions of the rest of the dataset. We will exclude outliers from our analysis, henceforth. After removing the outliers, we ended up with a dataset of 61142 asteroids. Figure 8 shows a joint plot and histograms of $g - r$ and $g - i$. Both distributions are single-peaked, slightly skewed, with skewness of -0.17 and -0.16, respectively, and leptokurtic, with kurtosis values of 3.37 and 3.08.

First, we investigate where asteroids in this new data set with known taxonomies could be located. Our results are shown in figure 9. We identified 71 asteroids with taxonomical data: 4 B-, 14 C-, 3 D-, 15 X-, 29 S-, 2 L-, and 3 V-types. B, C, D, and X asteroids are darker objects, associated with the so-called C-complex, while the other types are brighter objects associated with the S-complex. Our data show that the two complexes are fairly separated in this domain, with C-complex asteroids located in the left part of the ellipsoidal distribution of $(g - r, g - i)$ values, and S-complex asteroids concentrating in the right part. However, different taxonomies inside these complexes overlap with each other. While DES data could help discriminate between C- and S-complexes, we do not have enough resolution in the $(g - r, g - i)$ domain to perform a more in-depth taxonomical analysis, including the V-type asteroids.

To further confirm this hypothesis, we use the method of DeMeo & Carry (2013) to obtain taxonomical information for asteroids listed in the Sloan Digital Sky Survey-Moving Object Catalog data (SDSS-MOC4, Ivezić et al. 2001). Re-

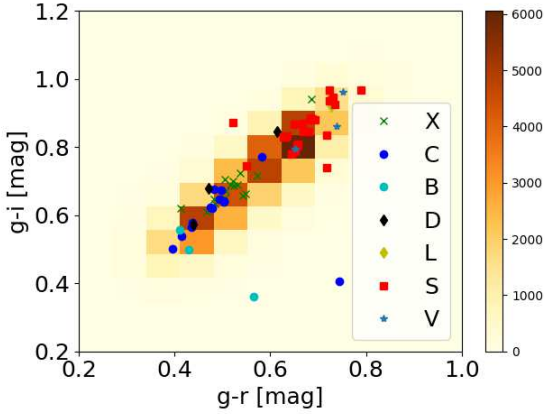


Figure 9. A 2D histogram in the $(g-r, g-i)$ plane of the asteroids with DES data. The color symbols are objects for which taxonomical information is available in the [Bus & Binzel \(2002\)](#), [Lazzaro et al. \(2004\)](#), and [DeMeo et al. \(2009\)](#) surveys, according to the color and size code shown in the legend.

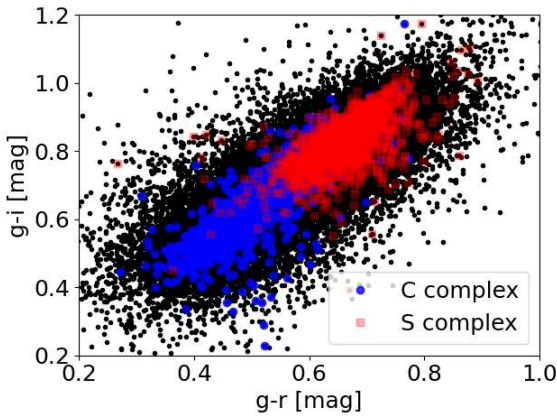


Figure 10. Projection in the $(g-r, g-i)$ plane of the asteroids with DES data and SDSS-MOC4 taxonomies. Blue circles identify asteroids likely to belong to the C-complex, while red squares display asteroids with more likely to belong to the S-complex. Black points are asteroids with no SDSS-MOC4 data.

sults for the [Carvano et al. \(2010\)](#) and [Popescu et al. \(2018\)](#) data sets are similar and will not be presented or discussed for the sake of brevity. We identify 3347 asteroids having data in both databases, of which 1514 are within the C-complex, and 1833 are within the S-complex. Figure 10 shows the $(g-r, g-i)$ distribution of these objects, which confirms the results from the spectroscopical surveys data: there is a clear separation between C-complex and S-complex asteroids in this domain. Again, the data resolution is not sufficient to distinguish between different asteroid types, as previously observed, and this is not shown in figure 10 for simplicity.

Finally, while the distribution of albedo values may vary among a single spectral type, C-complex asteroids tend to have lower values of geometric albedos p_V , while S-complex ones have larger p_V . We searched for objects in the DES dataset with albedo data in the WISE and NEOWISE, AKARI, or IRAS databases, and identified 5122 asteroids, as

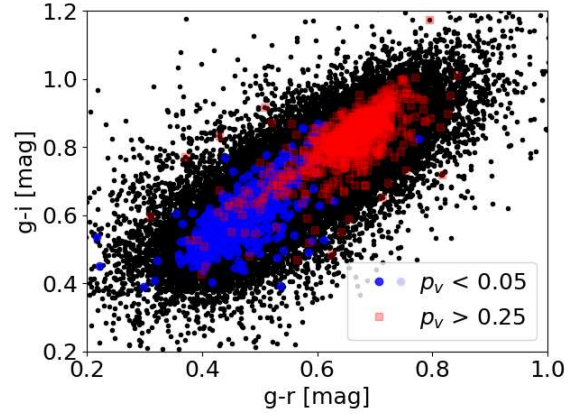


Figure 11. Projection in the $(g-r, g-i)$ plane of the asteroids with DES data and albedo values. Blue circles identify asteroids with albedo p_V lower than 0.05, while red squares display asteroids with $p_V > 0.25$.

shown in figure 11. While asteroids with intermediate albedos ($0.05 < p_V < 0.25$) cover the $(g-r, g-i)$ domain more or less uniformly, very dark ($p_V < 0.05$) and very bright ($p_V > 0.25$) asteroids are quite separated in the $(g-r, g-i)$ domain, which confirms the trends observed for taxonomic data.

Using taxonomic information obtained from the SDSS analysis, we utilized genetic algorithms to determine the optimal ML methods for predicting the complex type of asteroids based on the $(g-r, g-i)$ DES data. Our analysis found that the Linear Support Vector Classifier (Linear SVC, ([Cortes & Vapnik 1995](#))) performed the best.

Linear SVC is a type of machine learning algorithm used for classification tasks, where the goal is to assign each input to one of a set of predefined categories or classes. Linear SVC is a variant of the Support Vector Machine (SVM) algorithm that uses a linear kernel function. In Linear SVC, the algorithm tries to find the hyperplane that separates the different classes with the largest possible margin. The hyperplane is defined as the set of points in the feature space where the decision boundary between classes lies. The margin is the distance between the hyperplane and the closest points from each class. The larger the margin, the more robust the classification will be to noise and outliers.

For our model, we used a C parameter, which controls the trade-off between achieving a low training error and a low testing error, of 0.1. a penalty parameters equal to $l1$, which uses the $l1$ regularization method, and a tolerance parameter, which specifies the tolerance for stopping the optimization algorithm, of 0.0001. Other parameters were the standard choices for the Linear SVC algorithm. Our model achieved an accuracy of 90.9% on the validation set, which, as in the previous section, was 20% of the original training set.

Figure (12) shows predictions for 58118 new asteroids with no prior complex information. Our analysis suggests that 28871 of these objects belong to the C-complex, while 29247 are more likely to be S-complex asteroids. The higher fraction of S-complex asteroids, as opposed to C-complex in the $(g-r, g-i)$ domain with respect to the $(gri \text{ slope}, i-z)$ plane can be explained by the fact that, in the $(g-r, g-i)$

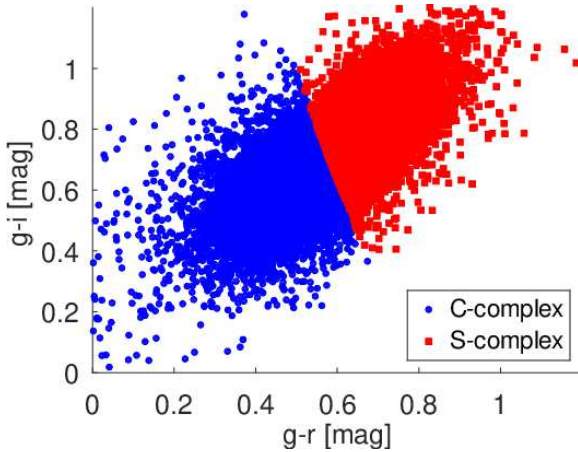


Figure 12. $(g-r, g-i)$ colors of the ML predicted data for asteroids in the DES database.

domain V-type asteroids are considered as part of the S-complex.

5 V-TYPE ASTEROIDS: DES CANDIDATES

In section (3), we observed that the accuracy of predicting V-type objects in the gri slopes and $i-z$ color plane was higher (65.6%) than for other classes. V-type objects are important because of their association with differentiated parent bodies and basaltic composition. Identifying their orbital location and physical properties may provide insights about the early phases of our Solar System formation. To date, asteroid 4 Vesta is the only confirmed differentiated body in the main belt, but other possible differentiated parent bodies have been suggested in the past. Using the DES data in the gri slopes and $i-z$ color plane, we identified 410 new potential V-type objects with available proper elements from the Asteroid Family Portal AFP, <http://asteroids.matf.bg.ac.rs/fam/> (Novaković et al. 2022), 85 of which are located in the central and outer main belt.

Figure (13) displays their projection onto a proper $(a, \sin(i))$ plane. The dynamical evolution of V-type objects suggests that there may be six possible regions where injected material, either from a local or remote source, can evolve due to non-gravitational forces. Carruba et al. (2014) identified three such regions in the central main belt, named after three possible local differentiated bodies: Hansa, Eunomia, and the Agnia/Merxia parent body. A similar analysis by Huaman et al. (2014) found three comparable dynamical regions in the outer main belt: the Dembowska, Eos, and Magnya regions. DES V-type candidates are primarily located where they are expected, near the Vesta family and in the densely populated Eunomia and Eos regions. Further investigation of their physical properties and understanding their dynamical evolution will remain a challenge for future studies.

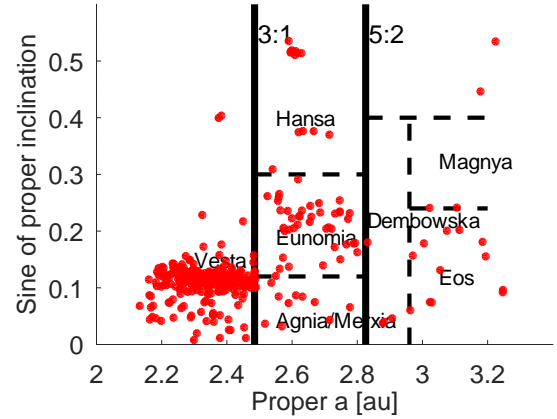


Figure 13. A proper $(a, \sin(i))$ projection of the V-type candidate asteroids identified using DES data. Vertical full lines identify the dynamical boundaries of the inner, central and outer main belt. The dashed lines show the location of the dynamical regions associated with possible local sources of V-type materials, as identified by Carruba et al. (2014) and Huaman et al. (2014).

6 SUMMARY AND CONCLUSIONS

In this study, we aimed to explore the feasibility of using DES data to infer physical properties of main belt asteroids. We initially focused on using the gri slopes and $i-z$ colors of asteroids, as this plane allows us to employ the taxonomic classification scheme of DeMeo & Carry (2013). After removing outliers, we identified a population of 17135 asteroids. However, with the exception of V-type and possibly C-type asteroids, DES data in this plane is insufficient to identify all the DeMeo & Carry (2013) taxonomies. Nonetheless, we can still distinguish between C- and S-complex taxonomies. We utilized machine learning approaches, optimized using genetic algorithms, to predict complex labels for 10213 asteroids that previously had no taxonomic information.

A much larger sample of objects is available if we consider the $(g-r, g-i)$ plane, with a sample of 61493 asteroids with such data obtained after outlier removal. We employed machine learning algorithms to predict the complex labels of 58118 new asteroids with no prior taxonomic information, using the asteroids with SDSS-MOC4 known taxonomies as a training sample.

Lastly, we used DES data to identify 410 possible new V-type objects. Their distribution in the proper $(a, \sin(i))$ domain is consistent with the location of known V-type bodies. Future research could concentrate on further examination of the physical characteristics and dynamical evolution of the asteroids identified in this study.

ACKNOWLEDGMENTS

We are grateful to an anonymous reviewer for insightful and constructive comments that greatly improved the quality of this work. We would like to thank the Brazilian National Research Council (CNPq, grant 304168/2021-1). J.I.B.C. acknowledges grants 305917/2019-6, 306691/2022-1 (CNPq) and 201.681/2019 (FAPERJ). This research used computational resources from the Interinstitucional Laboratory of e-Astronomy (LIneA) with financial support from the

INCT of the e-Universo (Process number 465376/2014-2). F.S.F. acknowledges the support of Coordenação de Aperfeiçoamento de Pessoal de Nível Superior - Brasil (CAPES) - Finance Code 001. V.F. acknowledges a CNPq support, PIBIC/ON (process 143944/2022-3). Funding for the DES Projects has been provided by the U.S. Department of Energy, the U.S. National Science Foundation, the Ministry of Science and Education of Spain, the Science and Technology Facilities Council of the United Kingdom, the Higher Education Funding Council for England, the National Center for Supercomputing Applications at the University of Illinois at Urbana-Champaign, the Kavli Institute of Cosmological Physics at the University of Chicago, the Center for Cosmology and Astro-Particle Physics at the Ohio State University, the Mitchell Institute for Fundamental Physics and Astronomy at Texas A&M University, Financiadora de Estudos e Projetos, Fundação Carlos Chagas Filho de Amparo à Pesquisa do Estado do Rio de Janeiro, Conselho Nacional de Desenvolvimento Científico e Tecnológico and the Ministério da Ciência, Tecnologia e Inovação, the Deutsche Forschungsgemeinschaft and the Collaborating Institutions in the Dark Energy Survey.

The Collaborating Institutions are Argonne National Laboratory, the University of California at Santa Cruz, the University of Cambridge, Centro de Investigaciones Energéticas, Medioambientales y Tecnológicas-Madrid, the University of Chicago, University College London, the DES-Brazil Consortium, the University of Edinburgh, the Eidgenössische Technische Hochschule (ETH) Zürich, Fermi National Accelerator Laboratory, the University of Illinois at Urbana-Champaign, the Institut de Ciències de l'Espai (IEEC/CSIC), the Institut de Física d'Altes Energies, Lawrence Berkeley National Laboratory, the Ludwig-Maximilians Universität München and the associated Excellence Cluster Universe, the University of Michigan, NSF's NOIRLab, the University of Nottingham, The Ohio State University, the University of Pennsylvania, the University of Portsmouth, SLAC National Accelerator Laboratory, Stanford University, the University of Sussex, Texas A&M University, and the OzDES Membership Consortium.

Based in part on observations at Cerro Tololo Inter-American Observatory at NSF's NOIRLab (NOIRLab Prop. ID 2012B-0001; PI: J. Frieman), which is managed by the Association of Universities for Research in Astronomy (AURA) under a cooperative agreement with the National Science Foundation.

The DES data management system is supported by the National Science Foundation under Grant Numbers AST-1138766 and AST-1536171. The DES participants from Spanish institutions are partially supported by MICINN under grants ESP2017-89838, PGC2018-094773, PGC2018-102021, SEV-2016-0588, SEV-2016-0597, and MDM-2015-0509, some of which include ERDF funds from the European Union. IFAE is partially funded by the CERCA program of the Generalitat de Catalunya. Research leading to these results has received funding from the European Research Council under the European Union's Seventh Framework Program (FP7/2007-2013) including ERC grant agreements 240672, 291329, and 306478. We acknowledge support from the Brazilian Instituto Nacional de Ciência e Tecnologia (INCT) do e-Universo (CNPq grant 465376/2014-2).

This manuscript has been authored by Fermi Research

Alliance, LLC under Contract No. DE-AC02-07CH11359 with the U.S. Department of Energy, Office of Science, Office of High Energy Physics.

7 DATA AVAILABILITY

The taxonomical complexes data, as well as the data on DES V-type candidates, are available at the NASA Planetary Data System (PDS): Carruba, V., Camargo, J. I. B., Aljbae, S., and the Dark Energy Survey Team (2024). Taxonomy, colors, and slope parameters for asteroids from the Dark Energy Survey V1.0. urn:nasa:pds:gbo.ast.des.taxonomy::1.0. NASA Planetary Data System; <https://doi.org/10.26033/m95p-bn08>.

8 CODE AVAILABILITY

All codes are available from the authors, upon reasonable request.

REFERENCES

- Abbott T. M. C., et al., 2021b, *The Astrophysical Journal Supplement Series*, 255, 20
- Abbott T. M. C., et al., 2021a, *ApJS*, 255, 20
- Banda-Huarcá M. V., et al., 2019, *AJ*, 157, 120
- Bernardinelli P. H., et al., 2021, *ApJ*, 921, L37
- Bernardinelli P. H., et al., 2022, *ApJS*, 258, 41
- Bernardinelli P. H., et al., 2023, [arXiv e-prints](https://arxiv.org/abs/2304.03017), p. [arXiv:2304.03017](https://arxiv.org/abs/2304.03017)
- Berthier J., Vachier F., Thuillot W., Fernique P., Ochsenbein F., Genova F., Lainey V., Arlot J. E., 2006, in Gabriel C., Arviset C., Ponz D., Enrique S., eds, *Astronomical Society of the Pacific Conference Series Vol. 351, Astronomical Data Analysis Software and Systems XV*. p. 367
- Blitzstein J. K., Hwang J., 2019, *Introduction to Probability*. CRC press
- Burke D. L., et al., 2018, *AJ*, 155, 41
- Bus S. J., Binzel R. P., 2002, *Icarus*, 158, 146
- Carrasco Kind M., Drlica-Wagner A., Koziol A., 2018, *easyaccess: SQL command line interpreter for astronomical surveys*, *Astrophysics Source Code Library*, record ascl:1812.008 (ascl:1812.008)
- Carruba V., Huaman M. E., Domingos R. C., Santos C. R. D., Souami D., 2014, *Monthly Notices of the Royal Astronomical Society*, 439, 3168
- Carruba V., Aljbae S., Domingos R. C., 2021, *Celestial Mechanics and Dynamical Astronomy*, 133, 24
- Carvano J. M., Hasselmann P. H., Lazzaro D., Mothé-Diniz T., 2010, *A&A*, 510, A43
- Chan T. F., Golub G. H., LeVeque R. J., 1979, Technical report, *Updating Formulae and a Pairwise Algorithm for Computing Sample Variances*. Stanford University, Stanford, CA, USA
- Chang C.-K., et al., 2019, *The Astrophysical Journal Supplement Series*, 241, 6
- Chen, P. W. and Wang, J. Y. and Lee H. 2004, in 2004 IEEE international joint conference on neural networks (IEEE Cat No04CH37541). pp 2035–2040
- Cortes C., Vapnik V., 1995, *Machine learning*, 20, 273
- Dark Energy Survey Collaboration et al., 2016, *MNRAS*, 460, 1270
- DeMeo F. E., Carry B., 2013, *Icarus*, 226, 723

- DeMeo F. E., Binzel R. P., Slivan S. M., Bus S. J., 2009, *Icarus*, **202**, 160
- Diehl H. T., et al., 2023, Technical Report FERMILAB-TM-2720-AE, The Dark Energy Survey and Operations: Year 6 – The Finale, <https://www.osti.gov/biblio/1596042/>. Fermi National Accelerator Lab. (FNAL), Batavia, IL (United States), <https://www.osti.gov/biblio/1596042/>
- Flaugher B., 2005, *International Journal of Modern Physics A*, **20**, 3121
- Flaugher B., et al., 2015, *The Astronomical Journal*, **150**, 150
- Gerdes D. W., et al., 2017, *ApJ*, **839**, L15
- Granvik M., Morbidelli A., Vokrouhlický D., Bottke W. F., Nesvorný D., Jedicke R., 2017, *A&A*, **598**, A52
- Huaman M. E., Carruba V., Domingos R. C., 2014, *MNRAS*, **444**, 2985
- Ivezić Ž., et al., 2001, *AJ*, **122**, 2749
- Ivezić Ž., et al., 2002, *AJ*, **124**, 2943
- Knežević Z., Milani A., 2003, *A&A*, **403**, 1165
- Lazzaro D., Angeli C. A., Carvano J. M., Mothé-Diniz T., Duffard R., Florczak M., 2004, *Icarus*, **172**, 179
- Masiero J. R., Mainzer A. K., Grav T., Bauer J. M., Cutri R. M., Nugent C., Cabrera M. S., 2012, *ApJ*, **759**, L8
- Milani A., Cellino A., Knežević Z., Novaković B., Spoto F., Paolichi P., 2014, *Icarus*, **239**, 46
- Morganson E., et al., 2018, *PASP*, **130**, 074501
- Novaković B., Vokrouhlický D., Spoto F., Nesvorný D., 2022, *Celestial Mechanics and Dynamical Astronomy*, **134**, 34
- Pan J., et al., 2022, *The Planetary Science Journal*, **3**, 269
- Popescu M., Licandro J., Carvano J. M., Stoicescu R., de León J., Morate D., Boacă I. L., Cristescu C. P., 2018, *A&A*, **617**, A12
- Pravec P., Harris A. W., Kušnirák P., Galád A., Hornoch K., 2012, *Icarus*, **221**, 365
- Radović V., Novaković B., Carruba V., Marčeta D., 2017, *MNRAS*, **470**, 576
- Roh D.-G., Moon H.-K., Shin M.-S., DeMeo F. E., 2022, *A&A*, **664**, A51
- Ryan E. L., Woodward C. E., 2010, *AJ*, **140**, 933
- Sabater J., Leon S., Verdes-Montenegro L., Sulentic J., Verley S., Boselli A., 2009, *A&A*, **494**, 693
- Stephens R., Warner B. D., 2018, in AAS/Division for Planetary Sciences Meeting Abstracts #50. p. 417.03
- Stephens R. D., Warner B. D., Harris A. W., 2010, in AAS/Division for Planetary Sciences Meeting Abstracts #42. p. 39.14
- Szabó G. M., Ivezić Ž., Jurić M., Lupton R., Kiss L. L., 2004, *MNRAS*, **348**, 987
- Usui F., et al., 2011, *PASJ*, **63**, 1117
- Warner B. D., Stephens R. D., Harris A. W., 2011, *Minor Planet Bulletin*, **38**, 172
- Willmer C. N. A., 2018, *ApJS*, **236**, 47

This paper has been typeset from a $\text{\TeX}/\text{\LaTeX}$ file prepared by the author.

This figure "ORCIDiD_icon16x16.png" is available in "png" format from:

<http://arxiv.org/ps/2311.03613v1>